IOP Publishing and International Atomic Energy Agency Nuclear Fusion
Nucl. Fusion **51** (2011) 012001 (4pp) doi:10.1088/0029-5515/51/1/012001

LETTER

Taming the plasma–material interface with the 'snowflake' divertor in NSTX

V.A. Soukhanovskii[1], J.-W. Ahn[2], R.E. Bell[3], D.A. Gates[3], S. Gerhardt[3], R. Kaita[3], E. Kolemen[3], B.P. LeBlanc[3], R. Maingi[2], M. Makowski[1], R. Maqueda[4], A.G. McLean[2], J.E. Menard[3], D. Mueller[3], S.F. Paul[3], R. Raman[5], A.L. Roquemore[3], D.D. Ryutov[1], S.A. Sabbagh[6] and H.A. Scott[1]

[1] Lawrence Livermore National Laboratory, Livermore, CA 94551, USA
[2] Oak Ridge Institute for Science and Education, Oak Ridge, TN 37831, USA
[3] Princeton Plasma Physics Laboratory, Princeton, NJ 08543, USA
[4] Nova Photonics, Inc., Princeton, NJ 08540, USA
[5] University of Washington, Seattle, WA 9819, USA
[6] Columbia University, New York, NY 10027, USA

E-mail: soukhanovskii2@llnl.gov

Received 7 October 2010, accepted for publication 24 November 2010
Published 16 December 2010
Online at stacks.iop.org/NF/51/012001

Abstract
Steady-state handling of divertor heat flux is a critical issue for ITER and future conventional and spherical tokamaks with compact high-power density divertors. A novel 'snowflake' divertor (SFD) configuration was theoretically predicted to have significant magnetic geometry benefits for divertor heat flux mitigation, such as an increased plasma-wetted area and a higher divertor volume available for volumetric power and momentum loss processes, as compared with the standard divertor. Both a significant divertor peak heat flux reduction and impurity screening have been achieved simultaneously with core H-mode confinement in discharges with the SFD using only a minimal set of poloidal field coils.

(Some figures in this article are in colour only in the electronic version)

The interface between a high-temperature plasma and a material surface is one of the outstanding challenges for magnetically confined fusion energy (MFE) research. A present vision of the plasma–material interface (PMI) for toroidal plasma devices (tokamaks) is a magnetic X-point divertor [1, 2]. In this concept, a region of open magnetic field lines surrounding the confined plasma (the scape-off layer (SOL)) is diverted away by additional divertor magnetic coils to a divertor chamber to minimize the interaction with vacuum vessel walls. The steady-state peak heat flux endured by the divertor chamber surface is limited by the present day divertor material and active cooling technology at $q_{pk} \leqslant 10\,\mathrm{MW\,m^{-2}}$. At higher heat fluxes the plasma facing component (PFC) lifetime and structural integrity are at risk due to increased material erosion rates and thermal stress. In the collisional SOL plasma, heat transport parallel to the field lines is often dominated by classical electron and ion conduction, whereas turbulence and intermittency set the cross-field heat and particle transport [1–4]. In order to reduce the power and particle fluxes exhausted in the divertor chamber, a number of solutions based on active techniques, e.g., impurity or D_2 seeded radiative divertors, field ergodization and strike point sweeping, and passive techniques, e.g., the number of divertors and divertor geometry, have been developed [1, 2]. These techniques aim to reduce the parallel heat flux $q_{\|}$ by volumetric power loss processes or SOL power partitioning, and reduce the heat flux q_{div} deposited on the PFCs by increasing the plasma-wetted surface area.

Spherical tokamaks (STs) impose even greater demands on divertor heat flux handling. The ST is viewed as a candidate concept for future fusion and nuclear science MFE devices [5–7]. Experiments in the National Spherical Torus Experiment (NSTX), a high-power density medium size ST ($R = 0.85\,\mathrm{m}$; $a = 0.65\,\mathrm{m}$) with graphite tile PFCs, have demonstrated the challenges of the inherently compact ST divertor: a large out/in SOL power ratio, a small divertor PFC area and reduced divertor volumetric (radiated power and momentum) losses. ITER-scale steady-state divertor heat fluxes $q_{pk} \leqslant 15\,\mathrm{MW\,m^{-2}}$ and $q_{\|} \leqslant 200\,\mathrm{MW\,m^{-2}}$ have been measured in $I_{\mathrm{p}} = 1.0$–$1.2\,\mathrm{MA}$ discharges heated by a 6 MW neutral beam injection (NBI) [8, 9]. While a successful reduction of divertor q_{pk} to 0.5–3 $\mathrm{MW\,m^{-2}}$ simultaneously

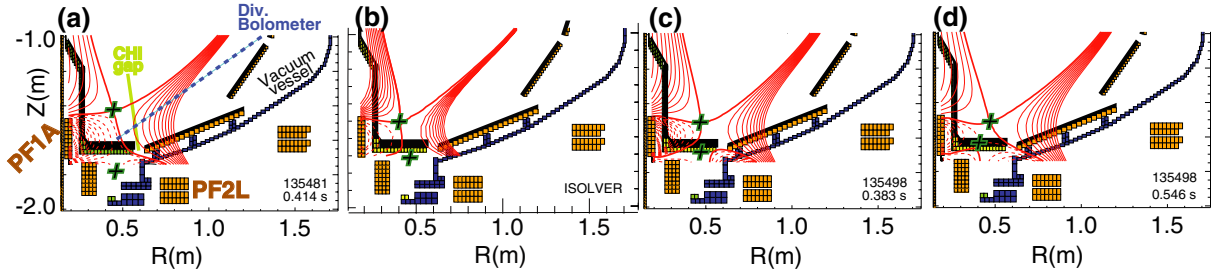

Figure 1. Poloidal magnetic flux equilibria for: (*a*) reference standard divertor configuration, with the divertor coils PF1A and PF2L, gap between divertor plates (CHI gap), and bolometer ch. 1 view shown; (*b*) modelled SFD-minus-like; experimental (*c*) SFD-minus-like and (*d*) SFD-plus-like configurations. Flux surfaces separated by 2 mm in the midplane are shown. Poloidal magnetic field nulls are shown by the green crosses.

with high (H-mode) core confinement has been demonstrated in NSTX with an additional divertor D_2 injection [9, 10], the radiative divertor technique alone is limited by the achievable divertor radiated power and does not scale favourably to future MFE devices (e.g. [6, 11]); thus, novel integrated approaches are sought.

Several innovative divertor geometries with attractive heat flux handling properties have been proposed recently [11–13]. One of them is a 'snowflake' divertor (SFD) configuration [13–16], which uses a second-order poloidal field null created by merging, or bringing close to each other, two first-order poloidal field null points (X-points) of a standard two-coil divertor configuration. A poloidal cross-section of the obtained magnetic flux surfaces with a hexagonal null-point has an appearance of a snowflake. The poloidal field B_p increases with distance as r^2 in the vicinity of the second-order null (versus r in the vicinity of a first-order null in the standard divertor), leading to (1) a higher divertor magnetic flux expansion $f_m = (B_p/B_{tot})_{MP}\,((B_p/B_{tot})_{SP})^{-1}$ (where B_{tot} is the total magnetic field at the strike point (SP) and midplane (MP) locations); (2) a higher plasma-wetted surface area $A_{wet} = 2\pi R_{SP} f_m \lambda_{q_{||}}$ (R_{SP} is the SP radius, and $\lambda_{q_{||}}$ is the MP (upstream) SOL power width) and (3) a longer X-point connection length L_x [14, 16]. The latter increases the heat diffusive loss into the private flux region, as well as the divertor volume available for impurity radiation and ion momentum losses. The SFD magnetic equilibria have been simulated for several tokamaks with existing divertor coils [15]. The SFD has already been realized in the TCV tokamak using a set of six divertor coils [17].

In this letter we present an experimental study of the SFD in NSTX. The SFD configuration for the first time (1) was obtained with a minimal number (two) of divertor coils; (2) resulted in a significant reduction of divertor q_{div} and $q_{||}$ leading to a partial detachment of the outer SP; (3) proved to be compatible with H-mode core confinement while demonstrating favourable impurity screening properties. Experimental results reported in this letter fully confirmed the theoretically predicted SFD properties [15, 16]. The two-coil SFD concept thus shows promise as a PMI solution for next-step high-power fusion devices that are likely to have few magnetic coils due to engineering and neutron constraints.

Magnetic control is critical for the SFD concept, since a second-order null configuration is topologically unstable [14, 16]. Two stable SFD-like configurations can be realized in practice: a SFD-plus, where the divertor coil currents slightly exceed those of the ideal SFD case, and a SFD-minus, where the corresponding divertor coil currents are slightly lower [14]. A predictive free-boundary axisymmetric Grad–Shafranov equilibrium code ISOLVER was used to model plasma equilibria with the SFD. The boundary shape, normalized pressure and current profiles from an existing medium triangularity discharge (similar to the one shown in figure 1(*a*)) were used to compute the plasma contribution to the flux ψ on a flux surface. The SFD was obtained by iteratively adjusting the currents in two divertor magnetic field coils PF1A and PF2L (also shown in figure 1(*a*)). Generally, the SFD-like configurations were generated when a secondary X-point was located on the flux surface within $\Delta\psi_N \leqslant 0.02$ from the separatrix (where normalized flux $\psi_N = 1$), and when a separation between the X-points in physical space was $d \leqslant 20$ cm (cf ion Larmor radius $r_L \leqslant 4$ mm). The corresponding deviation of the coil currents from those of the standard divertor was within 10–20%. (*a*) The standard divertor and (*b*) the modelled SFD-minus configurations are shown in figure 1. The benefits of the SFD are apparent from comparison of their magnetic geometry parameters shown in table 1.

Table 1. Typical geometry factors of the standard divertor, as well as the simulated and experimentally obtained SFD.

Quantity	Standard	Sim. SFD	Exp. SFD
Full connection length $L_{||}$ (m)	15–20	26	24–28
X-point to target connection length L_x (m)	5–10	10	10–20
Poloidal magnetic flux expansion f_m	10–24	60	40–100
Magnetic field angle at outer SP α (deg.)	1–2	∼1	∼1
Plasma-wetted area A_{wet} (m^2)	0.2–0.4	0.95	0.68–2.1

The ISOLVER model provided the PF1A and PF2L coil currents as well as the inner and outer SP coordinates for a practical implementation of the SFD in NSTX. In the experiment, the plasma control system (PCS) [18, 19] held the SP positions by real-time variation of the PF1A current for inner SP control, and the PF2L current for outer SP control. A proportional-integral-derivative (PID) controller algorithm with input from magnetic sensor and other diagnostic measurements was used [20]. The SFD-like configurations were obtained in a number of discharges for periods of 50–150 ms. Because of the time-dependent plasma inductance, ohmic transformer flux leakage, and variations in divertor structure eddy currents (none of which were included in the

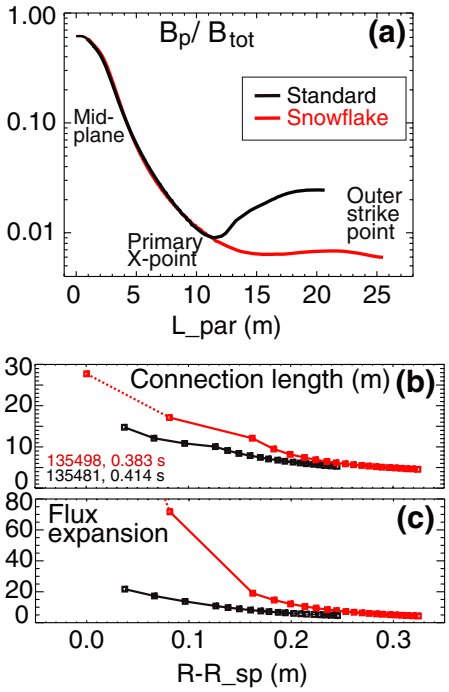

Figure 2. Comparison between the standard divertor and SFD (*a*) B_p/B_{tot} as a function of connection length $L_\parallel$ from MP to outer SP; (*b*) L_x and (*c*) f_m as functions of divertor major radius.

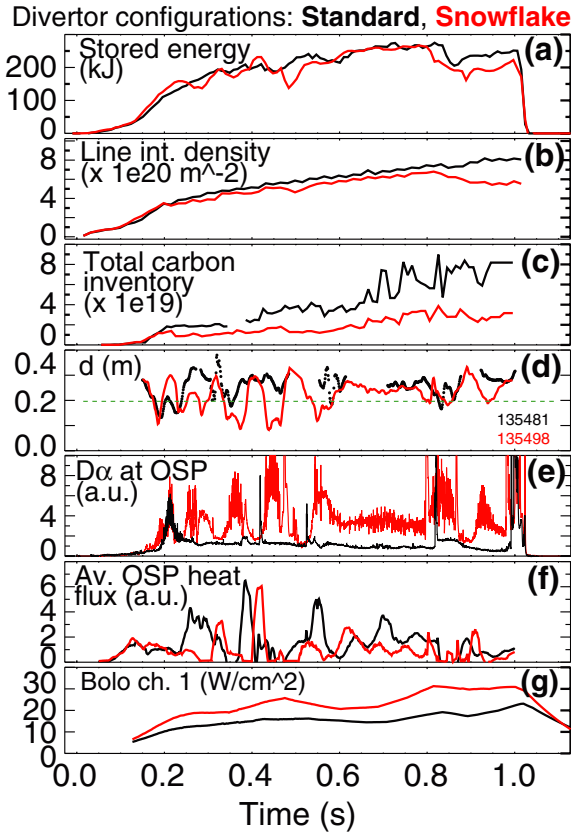

Figure 3. Time histories of core and edge plasma quantities in the standard divertor and the SFD discharges: (*a*) Stored energy W_{MHD}; (*b*) $\bar{n}_e$; (*c*) Core carbon inventory; (*d*) Divertor null-point separation *d*; (*e*) Divertor outer SP D_α intensity; (*f*) Average divertor outer SP region heat flux; (*h*) Plasma brightness from slow time response divertor bolometer chord shown in figure 1(*a*).

ISOLVER model), both d and $\Delta\psi_N$ changed in time, resulting in intermittent switching between the SFD and standard configuration. For example, the SFD discharge to be discussed below had five periods with the SFD-minus-like (figure 1(*c*)), and one with the SFD-plus-like (figure 1(*d*)) configurations. We are presently implementing an improved gain matrix in the PCS PID algorithm, and the real-time tracking and control of the second null-point in the NSTX PCS in order to maintain the SFD for an entire discharge duration (1–2 s).

Magnetic and plasma characteristics of the SFD were studied in discharges with $I_p = 0.8$ MA, $B_t = 0.4$ T, and 4–6 MW of NBI heating. Lithium coatings evaporated on PFCs in the amount of 80–100 mg per discharge were used for wall conditioning and plasma performance improvements [21, 22]. Two H-mode discharges with similar shaping ($\kappa \sim 1.9$–2.0 and $\delta \sim 0.6$–0.7) and SOL power $P_{SOL} \simeq 3$ MW, but with different divertor configurations (the standard divertor versus the SFD-minus) will be compared. Core and edge diagnostics used in this study are described elsewhere [9, 10].

The experimental magnetic equilibria confirmed the magnetic geometry properties of the SFD predicted by the ISOLVER model and analytic two-coil SFD theory [13, 14], as shown in table 1. The experimental equilibria were reconstructed with Grad–Shafranov equilibrium codes EFIT and LRDFIT using standard magnetic and kinetic constraints [23]. Divertor geometries of the standard and SFD discharges are compared in figure 2. The presence of a secondary null-point in the SFD reduced B_p/B_{tot} in the divertor separatrix region by up to 90%, as shown in figure 2(*a*). This increased the X-point connection length L_x by up to 50% and the flux expansion f_m (as well as A_{wet}) in the outer SP region by up to 90%. The radial divertor profiles of both L_x and f_m in figures 2(*b*) and (*c*) show that the geometry was modified in the SOL radial region near the separatrix ($\Delta = 2$–3 mm when mapped to MP using f_m), while similar magnetic properties were retained outside of this SOL region at large distances from the nulls in both discharges.

The SFD was found to be compatible with high confinement plasma operation, with no degradation in H-mode performance (figure 3(*a*)). In the standard divertor discharge, ELMs were suppressed as a result of lithium conditioning [24]. These ELM-free H-mode discharges had impurity accumulation leading to $Z_{eff} \sim 2$–4 from carbon and radiated power $P_{rad} = 1$–3 MW from metallic impurities after 0.5 s [25]. The SFD discharge in contrast showed exceptional impurity screening properties: the core carbon inventory N_c (as well as P_{rad}) was reduced by up to 75% leading also to a 10–15% reduction in n_e (figures 3(*b*) and (*c*)). The similarity of the carbon density and carbon concentration profiles (up to a scaling factor 1.5–2) suggested an edge carbon source reduction in discharges with the SFD.

Divertor measurements in the SFD [26] showed the commonly observed characteristics of divertor detachment [1, 2, 9, 10, 27]: an increase in divertor radiated power and electron–ion recombination rates, a loss of parallel pressure balance, and as a result, a decrease of heat and particle fluxes to the plate. A good correlation was observed between the SFD periods when the inter-null distance $d \leqslant 20$ cm (figure 3(*d*)) on the one hand, and the increases in the outer SP divertor D_α

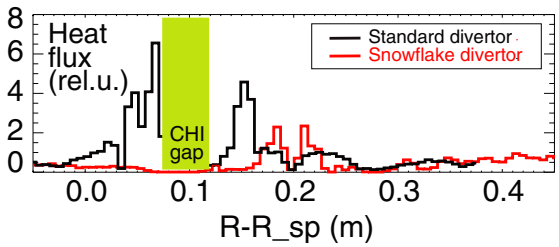

Figure 4. Relative divertor heat flux profiles in the standard divertor and SFD configurations.

intensity induced by volume recombination, significant drops in the divertor heat flux averaged over the radial region $\Delta = 15$ cm adjacent to the outer SP, on the other hand, as shown in figures 3(*e*) and (*f*). While the heat flux measurements were uncalibrated due to lithium coatings on divertor surfaces, typical $q_{pk} = 4$–$6\,\mathrm{MW\,m^{-2}}$ have been measured in similar standard divertor discharges. The averaged divertor heat flux was reduced in the SFD discharges by up to 30–40% due to increased divertor radiated power. The divertor bolometer signal indicative of divertor P_{rad} showed a 50% increase in the SFD versus the standard divertor (figure 3(*g*)).

Divertor peak heat fluxes q_{pk} were reduced by up to 90% in the detachment region adjacent to the separatrix ($\Delta = 2$–3 mm as mapped to MP with f_{m} taken into account), as shown in figure 4. In the attached SOL at $R_{\mathrm{div}} \geqslant 0.6$ m, similar divertor heat fluxes were measured in the SFD and the standard divertor, due to similar magnetic geometries. Taking the MP SOL width as $\lambda_{q_\parallel} \sim 6$–$7$ mm [28], we conclude that a significant fraction of divertor heat was exhausted through volumetric processes in the SFD. In the SFD discharges, spatially resolved Balmer spectra showed a formation of a large volume recombination region with average $T_{\mathrm{e}} \simeq 0.8$–$1.1$ eV and $n_{\mathrm{e}} \simeq (2$–$7) \times 10^{20}\,\mathrm{m^{-3}}$ [26] inferred from the modelling with the radiation transport and collisional–radiative code CRETIN [29]. A comparison of the inferred electron pressure in the SP region $p_{\mathrm{e}} = n_{\mathrm{e}}\,T_{\mathrm{e}} \sim 25$–$80$ Pa to the measured MP pressure $p_{\mathrm{e}} \sim 50$–120 Pa confirmed a pressure decrease from midplane to target in the SFD. In a partially detached divertor SP region with $T_{\mathrm{e}} \leqslant 1$–$2$ eV, a significant reduction of divertor physical and chemical sputtering rates, as well as an improved impurity entrainment in a hydrogenic plasma flow are expected [9, 10, 27, 30, 31]. While the physical mechanism is yet to be confirmed, this is consistent with the observed reduction in Z_{eff} and impurity concentration in the SFD discharges.

In previous NSTX divertor experiments q_{pk} showed a linear scaling with P_{SOL} and a weak dependence on n_{e} [10, 28]. The outer SP detachment did not occur in standard divertor configurations at the SOL power $1.5 \leqslant P_{\mathrm{SOL}} \leqslant 5$ MW, because of insufficient divertor carbon P_{rad}. The SOL power flow from the X-point to the divertor SP is described by $\nabla \cdot q_\parallel = S_E$, where S_E is a sum of volumetric energy sources and sinks, the latter being mainly due to volumetric divertor P_{rad} and ion-neutral charge exchange losses. The SFD magnetic properties significantly affected parallel divertor heat transport in the separatrix region by increasing collisionality and the divertor volume, and thus the volumetric losses. This led to a partial detachment of the outer SP, despite the counter-balancing effect of lithium conditioning that tended to reduce recycling and divertor n_{e}. In addition, the power deposited in the divertor was reduced due to the much-increased plasma-wetted area A_{wet}. Applying a simplified 1D model of electron conduction-dominated parallel heat transport with non-coronal carbon radiation (as discussed in [9, 10]), a 50% increase in L_x and divertor n_{e} is sufficient to increase carbon P_{rad} losses necessary to reduce $q_\parallel$ to a detachment level of 0.5–$1\,\mathrm{MW\,m^{-2}}$ [10]. This is also in qualitative agreement with the 2D multi-fluid modelling of the SFD heat transport in a DIII-D tokamak geometry [16].

In summary, the results of this letter provide support for the SFD concept as a promising solution of the PMI problem for next-step high-power fusion devices. We demonstrated that a SFD-like configuration could be obtained with only two existing divertor coils in NSTX, and in comparison with the standard divertor, it significantly reduced both parallel and deposited divertor heat fluxes and improved impurity screening, while maintaining H-mode confinement.

Acknowledgments

This work was performed under the auspices of the US Department of Energy under Contracts DE-AC52-07NA27344, DE-AC02-09CH11466, DE-AC05-00OR22725, W-7405-ENG-36 and DE-FG02-04ER54758. The entire NSTX Team is acknowledged for technical and operational support.

References

[1] ITER Physics Expert Group on Divertor *et al* 1999 *Nucl. Fusion* **39** 2391
[2] Loarte A. *et al* 2007 *Nucl. Fusion* **47** S203
[3] Leonard A. *et al* 1997 *Phys. Rev. Lett.* **78** 4769
[4] Hidalgo C. *et al* 2003 *Phys. Rev. Lett.* **91** 065001
[5] Peng Y.-K. *et al* 2005 *Plasma Phys. Control. Fusion* **47** 263
[6] Canik J. *et al* 2009 *J. Nucl. Mater.* **390–391** 315
[7] Goldston R. *et al* 2008 *Proc. 22nd Int. Conf. on Fusion Energy 2008 (Geneva, Switzerland, 2008)* CD-ROM file FT/P3-12 (Vienna: IAEA) http://www-naweb.iaea.org/napc/physics/FEC/FEC2008/html/node101.htm#23954
[8] Maingi R. *et al* 2003 *Plasma Phys. Control. Fusion* **45** 657
[9] Soukhanovskii V. *et al* 2009 *Nucl. Fusion* **49** 095025
[10] Soukhanovskii V.A. *et al* 2009 *Phys. Plasmas* **16** 022501
[11] Kotschenreuther M. *et al* 2007 *Phys. Plasmas* **14** 72502
[12] Valanju P. *et al* 2009 *Phys. Plasmas* **16** 056110
[13] Ryutov D. 2007 *Phys. Plasmas* **14** 64502
[14] Ryutov D. *et al* 2008 *Phys. Plasmas* **15** 092501
[15] Ryutov D. *et al* 2008 *Proc. 22nd Int. Conf. on Fusion Energy 2008 (Geneva, Switzerland, 2008)* (Vienna: IAEA) CD-ROM file IC/P4-8 http://www-naweb.iaea.org/napc/physics/FEC/FEC2008/html/node199.htm#43720
[16] Umansky M. *et al* 2009 *Nucl. Fusion* **49** 075005
[17] Piras F. *et al* 2009 *Plasma Phys. Control. Fusion* **51** 055009
[18] Ferron J. *et al* 1998 *Nucl. Fusion* **38** 1055
[19] Gates D. *et al* 2006 *Nucl. Fusion* **46** 17
[20] Kolemen E. *et al* 2010 *Nucl. Fusion* **50** 105010
[21] Kugel H.W. *et al* 2008 *Phys. Plasmas* **15** 056118
[22] Bell M. *et al* 2009 *Plasma Phys. Control. Fusion* **51** 124054
[23] Sabbagh S. *et al* 2001 *Nucl. Fusion* **41** 1601
[24] Maingi R. *et al* 2009 *Phys. Rev. Lett.* **103** 075001
[25] Canik J.M. *et al* 2010 *Phys. Rev. Lett.* **104** 045001
[26] Soukhanovskii V. *et al* 2011 *J. Nucl. Mater.* at press http://dx.doi.org/10.1016/j.jnucmat.2010.07.047
[27] Gruber O. *et al* 1995 *Phys. Rev. Lett.* **74** 4217
[28] Maingi R. *et al* 2007 *J. Nucl. Mater.* **363–365** 196
[29] Scott H. 2001 *J. Quant. Spectrosc. Radiat. Transfer* **71** 689
[30] Whyte D. *et al* 2001 *Nucl. Fusion* **41** 1243
[31] Bosch H.S. *et al* 1996 *Phys. Rev. Lett.* **76** 2499